Resonant Brillouin scattering in ZnSe

Sadao Adachi and Chihiro Hamaguchi

Department of Electronics, Osaka University, Suita, Osaka 565, Japan

(Received 5 July 1978)

Resonant Brillouin scattering in ZnSe has been investigated at room temperature and at 77 K by using the amplified acoustical-domain injection method. The observed dispersion curves have shown resonant cancellation and enhancement in the region near the fundamental absorption edge, and new maxima have been found in the scattering cross sections very close to the ground-state exciton energy region. The Brillouin-scattering cross section is found to depend strongly on the lifetime-broadening effect of the intermediate electronic states near the resonance region. The dispersion of the Brillouin-scattering cross section has shown good agreement with the theoretical analysis based upon Loudon's light scattering theory, assuming the virtual Wannier-Mott exciton transitions when the lifetime-broadening effect is taken into account. The dispersion curves of the photoelastic constants, $p_{11} - p_{12}$ and p_{44}, have been determined from the piezobirefringence analysis, where the lifetime-broadening effect is also taken into consideration as in the Brillouin-scattering analysis.

I. INTRODUCTION

In recent years theoretical and experimental investigations on the subject of resonant light scattering in semiconductors have been carried out extensively by many workers. The majority of the experimental studies have been concentrated on dispersion of the scattering cross section when the incident-photon energy approaches dielectric singularities of the semiconductors. The acoustoelectrically amplified phonon domains have recently been used to investigate resonant phenomena of the Brillouin scattering in piezoelectric semiconductors such as GaAs,[1] CdS,[2-5] ZnO,[3] and CdSe,[6] where the intense acoustical-phonon domains provide strong scattering signals and thus permit the use of a continuous light source monochromized by a conventional monochromator instead of a laser. This technique has also been extended by us to semiconductors with weak piezoelectricity such as ZnSe,[7] ZnTe,[8] and $Zn_xCd_{1-x}Te$,[9] by applying an acoustical-domain injection method.[10]

The dispersion of the Brillouin-scattering cross section in such semiconductors has shown resonant enhancement and cancellation (antiresonance) in the region near the fundamental absorption edge. The experimental dispersion curves are interpreted satisfactorily in terms of the resonant-light-scattering theory developed by Loudon.[11] However, resonant behaviors in the neighborhood of the exciton structure of the absorption edge , have not yet been discussed in detail because of the experimental difficulty due to the strong absorption coefficients in that wavelength region.

In this paper, we investigate resonant Brillouin scattering in ZnSe for slow TA ($T1$-mode) and fast TA ($T2$-mode) phonons in the wavelength ranges of 465–640 nm (room temperature) and 450–640 nm (77 K) which include a region sufficiently close to the fundamental absorption edge to clarify resonant behaviors near the M_0 critical point. Previous work by Ando *et al.*[7] is limited to the wavelength range of 475–620 nm (room temperature), and thus only a weak resonant enhancement is observed. We improved our experimental setup and used high-purity ZnSe, which enabled us to discuss the resonant behavior at a region very close to the fundamental absorption edge.

The experimental method is described in Sec. II. In order to obtain a strong phonon flux, the acoustical domains amplified in CdS have been transmitted into ZnSe through end-bonded surfaces by making use of the acoustical-domain injection method.[10] In Sec. III, we present the experimental results and compare with the theoretical model based upon Loudon's theory. The obtained dispersion of the Brillouin-scattering cross section shows a new scattering maximum at a photon energy very close to the ground-state exciton energy (in the resonant-enhancement region). We show for the first time that the scattering efficiency depends strongly on a lifetime-broadening effect of the intermediate electronic states. The importance of the broadening effect has been pointed out by Loudon[12] but not yet discussed from an experimental point of view. The maximum in the Brillouin-scattering cross section observed here is well interpreted by including this effect. In Sec. IV, we obtain the dispersion of the photoelastic constants $p_{11} - p_{12}$ and p_{44} from the present data by introducing the intrinsic piezobirefringence analysis as reported by Yu and Cardona.[13] From a macroscopic point of view, the Brillouin-scattering cross section is

proportional to the square of the photoelastic constant which can be obtained independently from the piezobirefringence experiment. We show that such a relation is valid even in the region of the fundamental absorption edge, which is justified from a microscopic point of view by taking the band structures of ZnSe into account. We also show here that the dispersion of the photoelastic constant (or piezobirefringence coefficient) depends strongly on the lifetime broadening of the electronic states in solids as in the case of Brillouin-scattering efficiency.

II. EXPERIMENTAL PROCEDURE

CdS single crystals used for generation and injection of the intense acoustical domains were purchased from Eagle-Picher Co. The resistivity and the electron mobility of CdS were about 30 Ω cm and 300 cm^2/V sec, respectively. ZnSe used in the present study was a melt-grown cubic, as-grown crystal. The crystal showed high resistivity ($\sim 10^9$ Ω cm) at room temperature.

CdS and ZnSe crystals were cut in the form of parallelepipeds with dimensions of about 0.6 $\times 1.5 \times 5.0$ mm. They were mechanically polished, and chemically etched at room temperature in a dilute HCl (CdS) and a HCl :HNO_3 = 1:1 mixture (ZnSe). Indium layers were deposited by vacuum evaporation onto the end-surfaces of CdS and ZnSe specimens, and they were bonded by heating the evaporated indium layers. The intense acoustical domain was produced by applying a pulse voltage across the CdS specimen, where the rod axis of CdS was perpendicular to the c axis, and the acoustical domain traveling along the rod axis was excited in CdS with atomic displacement parallel to the c axis. The indium layer made in such a way provided a high transmission efficiency of the acoustical domain from CdS into ZnSe specimen.[14] By way of example we obtained transmission efficiency up to 90% at 0.2-GHz phonon frequency. The details of this technique are described elsewhere.[10]

The specimen was set on a goniometer mounted on a rotatable table. The incident light obtained from a xenon flash tube was monochromized by a JASCO CT-50S grating monochromator and polarized

by a Gran-Thompson prism. The incident light was focussed by lenses, where the size of light spot was about 0.5 mm in diameter at the surface of the specimen. The scattered light was detected by a photomultiplier tube (RCA 7265) with a Polaroid HN 32 analyzer, and displayed on a storage oscilloscope (Tektronics 7623A). The experimental configurations of the Brillouin scattering-measurements for $T1$- and $T2$-mode phonons are listed in Table I. The measurements were made with the samples at room temperature and 77 K.

III. BRILLOUIN-SCATTERING CROSS SECTION

The dispersion of the Brillouin-scattering cross section for 0.2 GHz $T1$-mode phonon domains measured at room temperature is shown in Fig. 1. The Brillouin-scattering cross section shows a narrow and deep minimum at around 495 nm. Such an antiresonance behavior has also been found in GaAs,[1] CdS,[2-5] ZnO,[3] CdSe,[6] and ZnTe.[8] In addition, we can find a new scattering maximum in the dispersion curve very close to the fundamental absorption edge. Such a feature has not yet been found clearly in the previous work.[7]

The dispersion of the Brillouin-scattering cross section for 0.2 GHz $T2$-mode phonon domains measured at room temperature is shown in Fig. 2. The resonant feature observed here is essentially the same as that for the case of the scattering by the $T1$-mode phonon domains, but the cancellation point shifts slightly and occurs at 490 nm. As will be mentioned in Sec. IV, the resonant cancellation can be interpreted macroscopically in terms of the appropriate photoelastic constant passing through zero (isotropic point) while undergoing a reversal in sign (here we have to note that the scattering cross section is proportional to the square of the photoelastic constant). We can find a good agreement between the cancellation points observed from the scattering measurements and those (isotropic points) predicted from the piezobirefringence data (see Figs. 5 and 6).

A microscopic formulation of the resonant-light-scattering problem based on a third-order time-dependent perturbation was first given by Loudon.[11] In the theory, the following mechanism dominates for the resonant-light-scattering pro-

TABLE I. Experimental configurations for the Brillouin-scattering measurements.

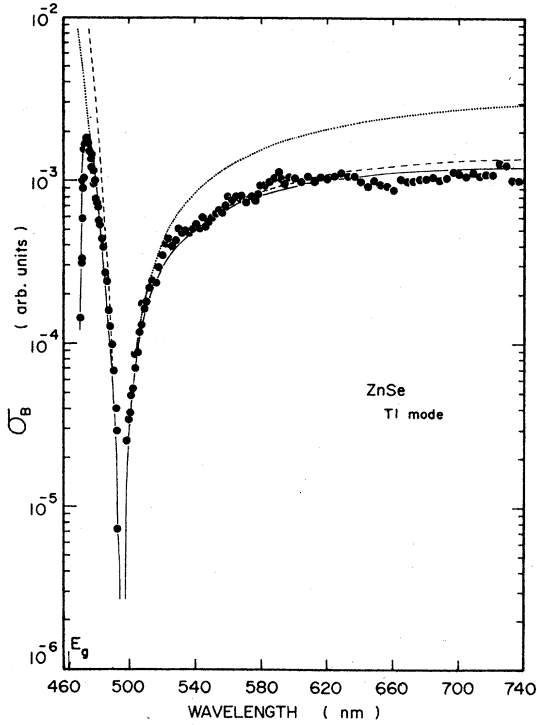| Acoustical mode	Acoustical propagation; I_K	Acoustical polarization; π	Incident light polarization; I_E	Scattered light polarization; I_S
$T1$ mode	$\vec{I}_K \parallel [1\bar{1}0]$	$\vec{\pi} \parallel [110]$	$\vec{I}_E \parallel [110]$	$\vec{I}_S \perp \vec{I}_E$
$T2$ mode	$\vec{I}_K \parallel [001]$	$\vec{\pi} \parallel [110]$	$\vec{I}_E \parallel [110]$	$\vec{I}_S \perp \vec{I}_E$

FIG. 1. Dispersion curves of the Brillouin-scattering cross section for 0.2 GHz T1-mode phonons measured at room temperature. The theoretical curves are obtained from Eq. (4) with $\Gamma = 0$ (dashed line) and $\Gamma = 64$ meV (solid line). The dotted line is obtained from Eq. (3). The vertical arrow indicates the position of the band gap E_g.
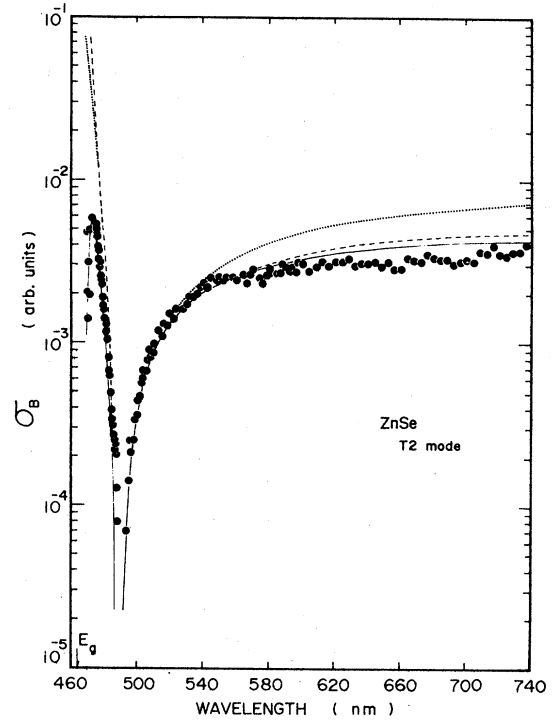

FIG. 2. Dispersion curves of the Brillouin-scattering cross section for 0.2 GHz $T2$-mode phonons measured at room temperature. The theoretical curves are obtained from Eq. (4) with $\Gamma = 0$ (dashed line) and $\Gamma = 56$ meV (solid line). The dotted line is obtained from Eq. (3). The vertical arrow indicates the position of the band gap E_g.

cess; a photon incident on a crystal creates a virtual electronic state (the free-electron–hole pair or the exciton state), the virtual electronic state is scattered by a phonon via a deformation-potential interaction, and finally the electronic state recombines to emit a scattered photon. The Brillouin-scattering cross section derived by Loudon has the following form:

$$\sigma_B = \left(\frac{e}{\hbar m c}\right)^4 \frac{\Phi}{2\rho v^2} \frac{\omega_s}{\omega_i} |R_{is}(-\omega_i, \omega_s, \omega_q)|^2, \qquad (1)$$

where ω_i and ω_s are the angular frequencies of the incident and the scattered light, respectively,

and Φ and ω_q are the energy density and the angular frequency of the relevant phonons. R_{is} is the frequency-dependent Brillouin (Raman) tensor. The corresponding frequencies are related by the energy conservation law

$$\omega_s = \omega_i \pm \omega_q . \qquad (2)$$

Modifying Loudon's result, we obtain the expression for the resonant-Brillouin term R_{is} in the case where the intermediate electronic state is assumed to be the free-electron–hole pair (for the spherical and parabolic bands) as[4]

$$R_{is} = \frac{2}{(2\pi)^2} \sum_{\alpha,\beta} \left(\frac{2\mu}{\hbar}\right)^{3/2} \frac{P_{0\beta}\Xi_{\beta\alpha}P_{\alpha 0}}{\omega_{g\beta} - \omega_{g\alpha} + \omega_q} \left[(\omega_{g\beta} - \omega_s)^{1/2} \tan^{-1}\left(\frac{\Delta\omega_\beta}{\omega_{g\beta} - \omega_s}\right)^{1/2} - (\omega_{g\alpha} - \omega_i)^{1/2} \tan^{-1}\left(\frac{\Delta\omega_\alpha}{\omega_{g\alpha} - \omega_i}\right)^{1/2}\right], \qquad (3)$$

and in the case for the Wannier-Mott exciton states[8,15] as

$$R_{is} = \sum_{\alpha,\beta} \frac{P_{0\beta}\Xi_{\beta\alpha}P_{\alpha 0}}{\omega_{g\beta} - \omega_{g\alpha} + \omega_q} \left(\frac{1}{\pi a_0^{*3}} \sum_n \frac{1}{n^3} \left(\frac{1}{(\omega_{g\alpha} - R^*/n^2 - \omega_i)} - \frac{1}{(\omega_{g\beta} - R^*/n^2 - \omega_s)}\right) + \frac{i}{4\pi}\left(\frac{2\mu}{\hbar}\right)^{3/2} (4\pi^2 R^*)^{1/2}\right.$$

$$\left. \times \left\{\left[1 - \exp-\left(-\frac{4\pi^2 R^*}{\omega_{g\alpha} - \omega_i}\right)^{1/2}\right]^{-1} - \left[1 - \exp-\left(-\frac{4\pi^2 R^*}{\omega_{g\beta} - \omega_s}\right)^{1/2}\right]^{-1}\right\}\right). \qquad (4)$$

In Eqs. (3) and (4), μ is the reduced mass which is assumed to be equal for the α and the β states for simplicity, $\Xi_{\beta\alpha}$ is the matrix element of deformation-potential scattering, $P_{0\beta}$ and $P_{\alpha 0}$ are the p matrix elements, where the subscript 0 indicates the electronic ground state and the subscripts α and β the intermediate electronic states. $\hbar\omega_{g\alpha}$ and $\hbar\omega_{g\beta}$ are the optical energy gaps for the incident and the scattered light, respectively, and $\hbar\Delta\omega_{\alpha}$ and $\hbar\Delta\omega_{\beta}$ stand for the values of combined widths of the energy bands. a_0^* and $\hbar R^*$ are the exciton Bohr radius and the exciton Rydberg constant, respectively. The first and the second terms on the right-hand side of Eq. (4) correspond to the nth discrete exciton and the unbound continuum exciton contributions, respectively. The resonant cancellation can be explained by the following equation[1]:

$$\sigma_B \propto |R_{is} + R_0|^2, \qquad (5)$$

where R_{is} is the resonant contribution given by Eq. (3) or (4), arising from the M_0 critical point, and R_0 is a nonresonant contribution arising from other, far-off critical points in the band structure. The resonant contribution R_{is} is opposite in sign to the nonresonant contribution R_0 in the longer-wavelength region (apart from the fundamental absorption edge). The cancellation therefore, occurs at a wavelength when $|R_{is} + R_0|$ becomes zero. As we shall see later, such a sign reversal relation does not hold in the region very close to the fundamental absorption edge when the lifetime-broadening effect is taken into account (see Figs. 3 and 4).

The intermediate electronic states produced by the incident radiation interact with the acoustical phonons via a deformation potential, resulting in a change in their electronic states. The transitions of the intermediate states are determined by the symmetry properties of the electronic states and the relevant phonon modes in crystals. Such a selection rule of the deformation-potential scattering determines the electronic transition process (two- or three-band process) which plays a dominant role in the resonant Brillouin process. The calculation of the matrix element $\Xi_{\beta\alpha}$ for the deformation-potential scattering has first been made by Ando and Hamaguchi in the case of wurtzite crystals like CdS.[4] In a similar way, we can calculate the matrix elements in the case of zinc-blende crystals like ZnSe using the corresponding orbital-strain Hamiltonian[16] and the wave functions for the s-like conduction and the p-like valence bands (at $\vec{k} = 0$) of zinc blende.[17] The results obtained for the nonzero matrix elements are as follows[7]:
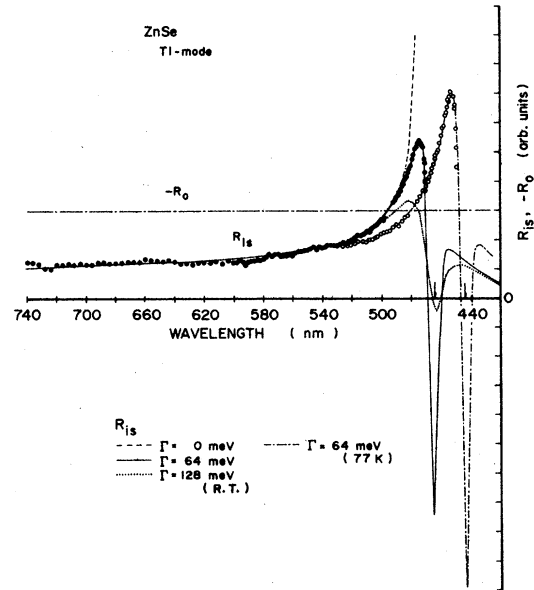

FIG. 3. Theoretical line shapes of R_{is} for the case of $T1$-mode phonons obtained from Eq. (4) with three different broadening parameters in the neighborhood of the exciton structure along with the experimental data measured at room temperature (solid circles) and 77 K (open circles). The vertical arrows indicate the positions of the lowest discrete exciton state E_{x1}. The corresponding nondispersive term $(-R_0)$ is also shown in the figure.
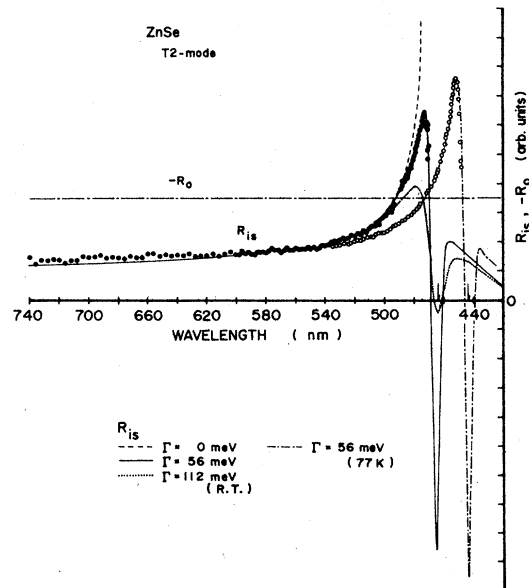

FIG. 4. Theoretical line shapes of R_{is} for the case of $T2$-mode phonons obtained from Eq. (4) with three different broadening parameters in the neighborhood of the exciton structure along with the experimental data measured at room temperature (solid circles) and 77 K (open circles). The vertical arrows indicate the positions of the lowest discrete exciton state E_{x1}. The corresponding nondispersive term $(-R_0)$ is also shown in the figure.

$\Xi_{BA} = 3^{1/2}b = 2.08$ eV, $\Xi_{CB} = 6^{1/2}b = 2.94$ eV,   (6)

for the $T1$-mode phonon scattering, and

$\Xi_{BA} = d = 3.81$ eV, $\Xi_{CB} = d/2^{1/2} = 2.69$ eV,

(7)

$\Xi_{CA} = 6^{1/2}d/2 = 4.67$ eV

for the $T2$-mode phonon scattering, where b and d are the shear deformation potentials[18] of the valence bands according to the notation of Picus and Bir,[16] and the subscripts A, B, and C indicate the Γ_8, Γ_8, and Γ_7 valence bands, respectively. From the above calculations, we can conclude that the intraband scattering in the valence bands (two-band process) and the scattering in the conduction band are forbidden for both the $T1$- and $T2$-mode acoustical phonons.

The theoretical curves obtained from Eqs. (3) and (4) are shown in Figs. 1 and 2 by dotted and dashed lines, respectively. The numerical values used in the calculations are listed in Table II. The curve calculated from Eq. (4) shows a better fit to the experimental data than that calculated from Eq. (3) except in the region very close to the ground-state exciton energy, where the theoretical dispersion shows a divergence. To remove the discrepancy we consider lifetime-broadening (i.e., damping) effect for the intermediate exciton states in Eq. (4). It is well known that the exciton transitions play an important role in the optical properties such as absorption and emission of photons in the band-edge spectral region, because the Coulomb interaction is always present between the electrons and the holes. They are affected strongly by the lifetime broadening especially at higher temperatures caused by the relatively strong coupling to LO phonons (thermal broadening). The lifetime-broadening effect can be introduced in Eq. (4) in a phenomenological manner by replacing ω by $\omega + i(\Gamma/2\hbar)$. As seen in Figs. 1 and 2, the theoretical dispersion exhibits a scattering peak near the band-edge region

when the lifetime-broadening effect is taken into account, and thus the fit shows an excellent agreement with the experimental data as shown by the solid lines. The best-fitting values of the broadening energy are determined to be $\Gamma = 64$ and 56 meV for the $T1$- and $T2$-modes, respectively.

Figures 3 and 4 show the theoretical line shapes of the Brillouin-tensor term R_{is} for the case of the $T1$- and the $T2$-mode phonons, respectively, calculated from Eq. (4) in the neighborhood of the exciton structure with different broadening energies. The experimental data $(\sigma_B^{1/2})$ measured at room temperature and 77 K are plotted in the figures by taking into account the corresponding nondispersive terms $-R_0$ which are also shown in the figures. When the exciton states have an infinite lifetime ($\Gamma = 0$), the theoretical dispersion of R_{is} shows a divergence near the band-edge region. The broadening effect depresses the resonant feature, and the scattering efficiency decreases with increasing broadening energy Γ. Consequently, the peak of the scattering efficiency appears in the resonant-enhancement region. The broadening energies determined in the present work do not depend on the temperature as clearly seen in Figs. 3 and 4. In general, the broadening energy can be expressed by a sum of the three different contributions

$$\Gamma(T) = \Gamma_0 + \Gamma_{ac}(T) + \Gamma_{LO}(T), \qquad (8)$$

where Γ_0 is independent of the temperature T, arising mainly from the impurity damping, Γ_{ac} is a contribution from acoustical phonons, proportional to T for low T, and Γ_{LO} is a contribution from LO phonons, proportional to $[\exp(\hbar\omega_{LO}/k_BT) - 1]^{-1}$ (here $\hbar\omega_{LO}$ is a LO phonon energy). Thus, $\Gamma(T)$ decreases with decreasing T. In the present case, the amplified acoustical domains have an energy density a factor of the order of 10^9 above the thermal equilibrium value, and thus Γ_{ac} has an appreciable value to contribute to the lifetime broadening. We can, therefore, expect specific

TABLE II. Parameters used to calculate the dispersion of the Brillouin-scattering cross section (eV). (i) Scattering of the holes between the A and B valence band (deformation potential matrix element Ξ_{BA}). (ii) Scattering of the holes between the B and C valence band (deformation potential matrix element Ξ_{CB}). (iii) Scattering of the holes between the A and C valence band (deformation potential matrix element Ξ_{CA}).

		$T1$ mode (0.2 GHz)				$T2$ mode (0.2 GHz)		
	$\hbar\omega_{gi}$	$\hbar\omega_{gs}$	$\hbar\Delta\omega_{\alpha,\beta}$	$\Xi_{\beta\alpha}$[b]	$\hbar\omega_{gi}$	$\hbar\omega_{gs}$	$\hbar\Delta\omega_{\alpha,\beta}$	$\Xi_{\beta\alpha}$[b]
(i)	2.68[a]	2.68	5.0	2.08	2.68	2.68	5.0	3.81
(ii)	2.68	3.09[a]	5.0	2.94	2.68	3.09	5.0	2.69
(iii)	⋯	⋯	⋯	⋯	2.68	3.09	5.0	4.67

[a] Reference 28.
[b] Reference 18.

effects on the lifetime broadening by the high-density acoustical phonons as also suggested by Segall,[19] and can conclude that the broadening mechanism arises mainly from the Γ_0 and Γ_{ac} contributions because of the temperature-independent nature of Γ.[20]

It should be noted here that the theoretical line shapes of R_{is} (solid lines) predict resonant cancellations at two different wavelengths [e.g., at 495 and 470 nm for the $T1$-mode (room temperature)] according to the relation given in Eq. (5). Such a feature has been found clearly in the present experiments as shown in Figs. 1 and 2. The theoretical curve, further, predicts that a strong scattering signal should be observed at wavelengths near the ground-state exciton energy region (due to sharp peaks, appeared in Figs. 3 and 4). We were, however, unable to find such a scattering signal because of the strong absorption coefficients in the exciton energy region. In spite of such difficulty in experiments, we believe that measurements are possible if sufficiently thin samples are prepared, and a continuously tunable dye laser is used in the Brillouin-scattering experiments. When the incident-photon energy approaches the exciton resonance, we have to take into account the excitonic polariton states in the Brillouin-scattering process. Brenig, Zeyher, and Birman[21] reported a theoretical analysis of the resonant Brillouin scattering in crystals exhibiting spatial dispersion which included excitonic polaritons as the intermediate states in the scattering process. Their result predicts a multiplet of the Brillouin spectrum near the exciton resonance with line separations and efficiencies, depending strongly on the incident-light energy because of the polariton dispersion. Recently, the first experimental observation of the effects predicted by Brenig et al. was reported by Ulbrich and Weisbuch in the Brillouin spectrum of GaAs,[22] and subsequently by Winterling and Koteles in CdS.[23] More recently, Bruce and Cummins observed resonant dispersion of the Brillouin shift in CdS with a high-resolution triple-pass Fabry-Perot interferometer.[24]

IV. PHOTOELASTIC CONSTANT

The purpose of Sec. IV is to determine spectral dependence of the photoelastic constants $p_{11} - p_{12}$ and p_{44}, which are involved in the Brillouin scattering from the $T1$- and the $T2$-mode acoustical phonons, respectively. The Brillouin-scattering cross section is proportional to the square of the relevant photoelastic constant. The value of the

photoelastic constants can be determined independently from the stress-induced birefringence (piezobirefringence, PB). The dispersion of the photoelastic constants derived here will be analyzed from the PB theory and compared with the PB data as reported by Yu and Cardona.[13]

The PB coefficients α defined by Higginbotham et al.[25] are related to the photoelastic constants by the following equations:

$$\alpha_{[001]} = (\Delta\epsilon_\parallel - \Delta\epsilon_\perp)/X = -\epsilon_{11}^2(p_{11} - p_{12})(S_{11} - S_{12})$$

$$(9)$$

for [001] stress direction, and

$$\alpha_{[111]} = (\Delta\epsilon_\parallel - \Delta\epsilon_\perp)/X = -\epsilon_{11}^2 p_{44} S_{44} \qquad (10)$$

for [111] stress direction, where $\Delta\epsilon_\parallel$ and $\Delta\epsilon_\perp$ are the change in the dielectric constants parallel and perpendicular to the direction of the stress X, ϵ_{11} is the component of the dielectric constant tensor in the absence of the stress, and S_{mn} is the component of the elastic compliance tensor. We can find from the macroscopic analysis of the Brillouin scattering given by Benedek and Fritsch[26] that the following simple relations exist:

$$\sigma_B(T1) \propto (p_{11} - p_{12})^2, \qquad (11)$$

$$\sigma_B(T2) \propto p_{44}^2. \qquad (12)$$

The first-order change in the real part of the dielectric constant with uniaxial stress can be expressed by

$$\Delta\epsilon_r(\omega) = \sum_{i=A,B,C} \left(\frac{\partial\epsilon_r}{\partial M_i}\Delta M_i + \frac{\partial\epsilon_r}{\partial\omega_{gi}}\Delta\omega_{gi}\right), \qquad (13)$$

where $M = |\langle|p|\rangle|^2$ is the squared p matrix element, and the summation indicates that contributions from the three valence bands must be included. The first and the second terms on the right-hand side of Eq. (13) correspond to the contribution from the first-order change in the squared p matrix elements and the interband transition energies, respectively. It is noteworthy that the expression given in Eq. (13) is analogous to that of the Brillouin-scattering efficiency in the quasi-static approximation,[27] where the phonons are assumed to act like static perturbations of the electronic band structure. Microscopic expression of the PB coefficient based on Eq. (13) has been given by Higginbotham et al.[25] by taking into account the E_0, $E_0 + \Delta_0$, E_1, $E_1 + \Delta_1$, and E_2 transitions. Applying their result to the present case, we obtain the photoelastic constant in the following form:

$$p_{11} - p_{12}(\text{or } p_{44}) = \frac{C}{\epsilon_{11}^2}\left\{ -g\left(\frac{\omega}{\omega_0}\right) + 4\frac{E_0}{\Delta_0}\left[f\left(\frac{\omega}{\omega_0}\right) - \left(\frac{\omega}{\omega_{0s}}\right)^{3/2} f\left(\frac{\omega}{\omega_{0s}}\right)\right]\right\}$$

$$+ \frac{C_{ex}}{\epsilon_{11}^2}\left\{ \frac{3 - \chi_{ex}^2}{(1 - \chi_{ex}^2)^2} + \frac{E_{ex}}{\Delta_0}\left[\frac{1}{1 - \chi_{ex}^2} - \left(\frac{E_{ex}}{E_{ex} + \Delta_0}\right)^3 \frac{1}{1 - \chi_{ex\ s}^2}\right]\right\} + D \,, \tag{14}$$

where

$$f(x) = [2 - (1+x)^{1/2} - (1-x)^{1/2}]/x^2 \,, \tag{15a}$$

$$g(x) = [2 - (1+x)^{-1/2} - (1-x)^{-1/2}]/x^2 \,, \tag{15b}$$

$$C = -\left(\tfrac{3}{2}m_e^*\right)^{3/2} P^2 b\,\omega_0^{-5/2} \quad \text{for } p_{11} - p_{12} \,,$$

$$C = -\tfrac{1}{4}\left(\tfrac{3}{2}m_e^*\right)^{3/2} P^2 d\,\omega_0^{-5/2} \quad \text{for } p_{44} \,, \tag{16a}$$

and

$$C_{ex} = -3(4\pi N f_1)b/E_{x1}^3 \quad \text{for } p_{11} - p_{12} \,,$$

$$C_{ex} = -3(4\pi N f_1)d/4E_{x1}^3 \quad \text{for } p_{44} \,. \tag{16b}$$

In Eqs. (14)–(16), $\hbar\omega$ is the photon energy, Δ_0 is the spin-orbit splitting energy,

$$\hbar\omega_0 = E_0 \,, \quad \hbar\omega_{0s} = E_0 + \Delta_0 \,, \quad \chi_{ex} = \hbar\omega/E_{x1} \,,$$

$$\chi_{ex\ s} = \hbar\omega/(E_{x1} + \Delta_0) \,,$$

E_{x1} is the ground-state exciton energy, P is the p matrix element, b and d the deformation po-

tentials of Picus and Bir,[18] and N and f_1 are the number of molecules per unit volume and the oscillator strength of the excitons, respectively. The first and the second terms in Eq. (14) correspond to the contribution from the band-to-band and the discrete exciton transitions, respectively. Since the contribution from the E_1, $E_1 + \Delta_1$, and E_2 gaps are generally less dispersive than those from the E_0 and $E_0 + \Delta_0$ gaps, we include such contributions in Eq. (14) as a nondispersive term D.

Figures 5 and 6 show the theoretical dispersion of $p_{11} - p_{12}$ and p_{44}, respectively, calculated from Eq. (14) along with the experimental data. The numerical values used to calculate the dispersion are listed in Table III. The PB data of Yu and Cardona[13] are also shown in the figures by the closed circles. As seen in the figures, the data obtained from the Brillouin scattering show quite good agreement with the PB data. The theoretical curve ($\Gamma = 0$) shows a poor fit with the experimental
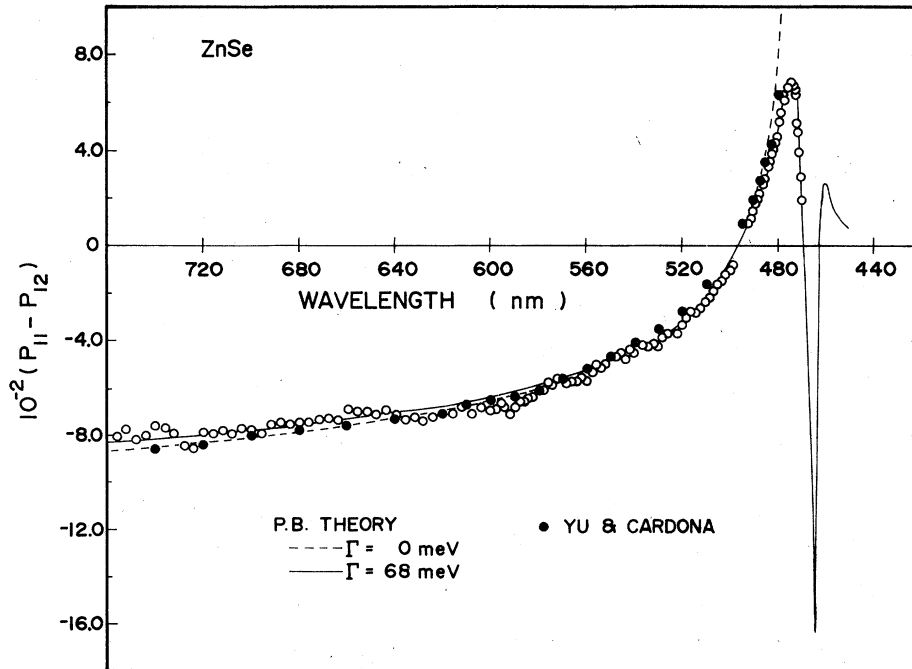

FIG. 5. Dispersion of the photoelastic constant $p_{11} - p_{12}$ (room temperature). Theoretical curves were obtained from Eq. (14) with $\Gamma = 0$ (dashed line) and $\Gamma = 68$ meV (solid line). The results of Yu and Cardona (Ref. 13) are also shown by the solid circles. PB theory stands for the piezobirefringence theory (see text).
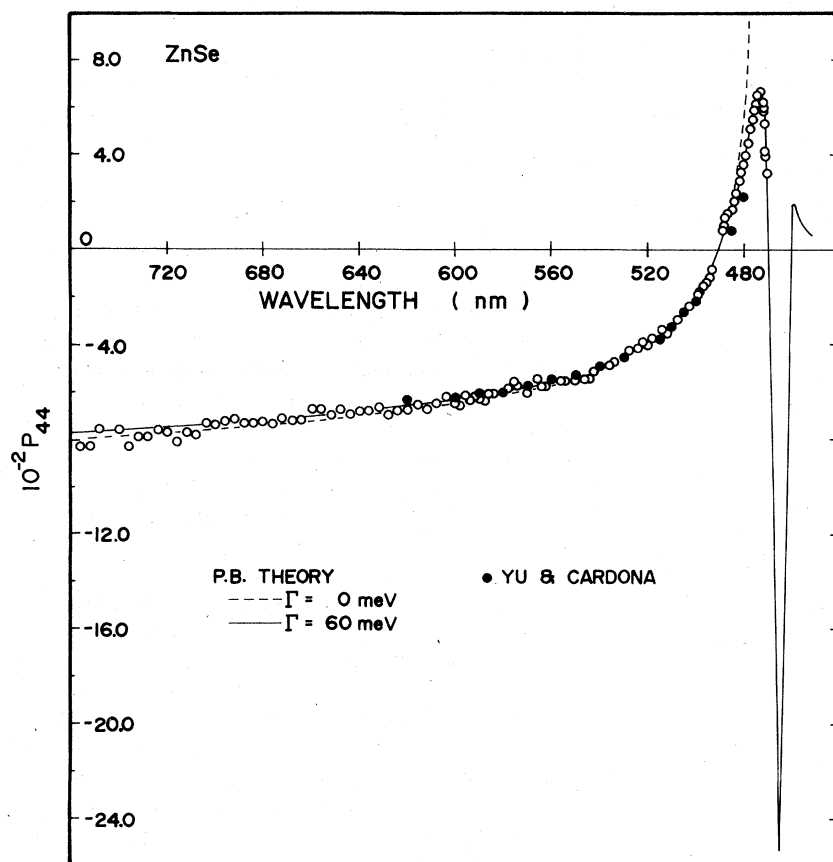
FIG. 6. Dispersion of the photoelastic constant p_{44} (room temperature). Theoretical curves were obtained from Eq. (14) with $\Gamma = 0$ (dashed line) and $\Gamma = 60$ meV (solid line). The results of Yu and Cardona (Ref. 13) are also shown by the solid circles. PB theory stands for the piezo-birefringence theory (see text).

data in the region near the fundamental absorption edge. Such a feature is improved by taking account of the lifetime-broadening effect as discussed earlier. This effect has not yet been considered in the previous PB analyses because of the experimental difficulty in the region of the photon energies sufficiently close to the fundamental absorption edge (where there exists strong absorption of light in thick samples used to avoid a destruction with applied uniaxial stress). The best-fitting values of the broadening energy are determined to be $\Gamma = 68$ and 60 meV for $p_{11} - p_{12}$ and p_{44}, respectively. These values agree

TABLE III. Numerical values used to calculate dispersion of the photoelastic constants.

	$p_{11} - p_{12}$	p_{44}
C [a]	1.42	9.15×10^{-1}
C_{ex} [a]	3.94×10^{-3}	5.26×10^{-3}
D [b]	-1.49×10^{-1}	-1.35×10^{-1}
$\epsilon_{11}(\omega)$	Ref. 34	Ref. 34

[a] Reference 13.
[b] Estimated from our experimental data.

reasonably with those derived in the analysis of the Brillouin-scattering cross section.

It can be seen that the line shape of the photoelastic constant (PB theory) is very similar to that of R_{is}. In addition, when the lifetime-broadening effect is taken into account in the resonant-light-scattering and the PB analyses, we find that they are equivalent to the line shape of the first-derivative modulation spectroscopy such as the thermoreflectance,[28] the wavelength modulation,[29,30] and the piezoreflectance.[31,32] The light scattering as a form of the modulation spectroscopy has been discussed in detail by Cardona[33] and Pinczuk and Burstein,[27] and such a treatment is usually referred to as the quasistatic approximation.[27] In a technique of the thermoreflectance spectroscopy, the modulation of a temperature results in a change in the optical property of the sample which is induced by a shift of the energy gaps and/or by a small change of the broadening parameter. Similar effect can also be expected in the case of the piezoreflectance spectroscopy. The resonant Brillouin-tensor term R_{is} is given by the first derivative of the model dielectric constant (with respect to the band-gap energy)

which is found to be equivalent to the change in the dielectric constant for the first-derivative modulation spectroscopy. Recently, indeed, we have found experimentally that the dispersion of the Brillouin-scattering cross section (R_{is}) is in quite good agreement in form with the spectrum obtained in the first-derivative modulation spectroscopy. Details will be published in the near future.

V. CONCLUSION

The Brillouin-scattering cross sections have shown a strong dependence on the lifetime broadening of the intermediate electronic states near the exciton resonance region. The experimental dispersion has been well interpreted in terms of the Loudon's light-scattering theory assuming virtual Wannier-Mott exciton transitions and including the lifetime-broadening effect. The dispersion of the photoelastic constants $p_{11}-p_{12}$ and p_{44} has been determined by introducing the piezobirefringence analysis where the lifetime-broadening effect is also taken into consideration as in the case of Brillouin-scattering analysis. It is found from the present analyses that the dispersion curves of the Brillouin-scattering cross section and the photoelastic constant are well interpreted by taking the band structures of ZnSe into account. The broadening energy, which arises mainly from the temperature-independent part of the broadening mechanism, has been determined from Brillouin-scattering and piezobirefringence analyses as $\Gamma \simeq 60$ meV.

[1] D. K. Garrod and R. Bray, Phys. Rev. B 6, 1314 (1972).

[2] U. Gelbart and A. Many, Phys. Lett. A 43, 329 (1973).

[3] R. Berkowicz and T. Skettrup, Phys. Rev. B 11, 2316 (1975).

[4] K. Ando and C. Hamaguchi, Phys. Rev. B 11, 3876 (1975).

[5] S. Adachi and C. Hamaguchi, J. Phys. Soc. Jpn. 45, 505 (1978).

[6] K. Yamamoto, K. Misawa, H. Shimizu, and K. Abe, J. Phys. Chem. Solids 37, 181 (1976).

[7] K. Ando, K. Yamabe, S. Hamada, and C. Hamaguchi, J. Phys. Soc. Jpn. 41, 1593 (1976).

[8] S. Adachi and C. Hamaguchi, J. Phys. Soc. Jpn. 43, 1637 (1977).

[9] S. Adachi and C. Hamaguchi, J. Phys. Soc. Jpn. 44, 343 (1978).

[10] K. Yamabe, K. Ando, and C. Hamaguchi, Jpn. J. Appl. Phys. 16, 747 (1977).

[11] R. Loudon, Proc. R. Soc. London, Ser. A 275, 218 (1963).

[12] R. Loudon, J. Phys. (Paris) 26, 677 (1965).

[13] P. Y. Yu and M. Cardona, J. Phys. Chem. Solids 34, 29 (1973).

[14] C. Hamaguchi, K. Yamabe, K. Ando, and S. Adachi, in Proceedings of the Sixth International Conference on Internal Friction and Ultrasonic Attention in Solids, edited by R. R. Hasiguti and N. Mikoshiba (University of Tokyo, Tokyo, 1977), p. 183.

[15] A. K. Ganguly and J. L. Birman, Phys. Rev. 162, 806 (1967).

[16] G. E. Picus and G. L. Bir, Fiz. Tverd. Tela. 1, 154 (1959) [Sov. Phys. Solid State 1, 136 (1959)].

[17] F. H. Pollak and M. Cardona, Phys. Rev. 172, 816 (1968).

[18] D. W. Langer, R. N. Euwema, K. Era, and T. Koda, Phys. Rev. B 2, 4005 (1970).

[19] B. Segall, in Proceedings of the International Conference on the Physics of Semiconductors (Nauka, Lenin-grad, 1968), Vol. 1, p. 425.

[20] In order to obtain a perfect crystal, we have tried the Zn-extraction method [G. E. Hite, D. T. F. Marple, M. Aven, and B. Segall, Phys. Rev. 156, 850 (1967)]. The best-fitting value of the Brillouin-scattering cross section for Zn-extracted ZnSe was determined as $\Gamma = 44$ meV at room temperature and also 77 K. This fact indicates that the lifetime broadening arises, at least, from the Γ_0 part. A similar conclusion has also been reached for ZnTe. Detailed study is in progress to determine the origin of this mechanism.

[21] W. Brenig, R. Zeyher, and J. L. Birman, Phys. Rev. B 6, 4617 (1972).

[22] R. G. Ulbrich and C. Weisbuch, Phys. Rev. Lett. 38, 865 (1977).

[23] G. Winterling and E. Koteles, Solid State Commun. 23, 95 (1977).

[24] R. H. Bruce and H. Z. Cummins, Phys. Rev. B 16, 4462 (1977).

[25] C. W. Higginbotham, M. Cardona, and F. H. Pollak, Phys. Rev. 184, 821 (1969).

[26] G. B. Benedek and K. Fritsch, Phys. Rev. 149, 647 (1966).

[27] A. Pinczuk and E. Burstein, in Light Scattering in Solids, edited by M. Cardona (Springer, Berlin, 1975), p. 23.

[28] E. Matatagui, A. G. Thompson, and M. Cardona, Phys. Rev. 176, 950 (1968).

[29] A. N. Georgobiani, Yu. V. Ozerov, and H. Friedrich, Fiz. Tverd. Tela. 15, 2986 (1973) [Sov. Phys. Solid State 15, 1991 (1974)].

[30] A. N. Georgobiani, Yu. V. Ozerov, and H. Friedrich, Phys. Status Solidi B 68, 663 (1975).

[31] W. E. Engeler, H. Fritzsche, M. Garfinkel, and J. J. Tiemann, Phys. Rev. Lett. 14, 1069 (1965).

[32] H. Mathieu, J. Camassel, and D. Auvergne, Phys. Status Solidi B 68, 797 (1975).

[33] M. Cardona, Surf. Sci. 37, 100 (1973).

[34] D. T. F. Marple, J. Appl. Phys. 35, 539 (1964).